Human Molecular Genetics, 2017, Vol. 26, No. 21 4105–4117

doi: 10.1093/hmg/ddx298
Advance Access Publication Date: 26 July 2017
Original Article

ORIGINAL ARTICLE

The NAD$^+$-dependent deacetylase SIRT2 attenuates oxidative stress and mitochondrial dysfunction and improves insulin sensitivity in hepatocytes

Vera Lemos[1,†], Rita M. de Oliveira[2], Luana Naia[3], Éva Szegö[4], Elisabete Ramos[5,6], Sónia Pinho[7], Fernando Magro[1], Cláudia Cavadas[3,8], A. Cristina Rego[3,9], Vítor Costa[10,11,12], Tiago F. Outeiro[2,4] and Pedro Gomes[1,3,*]

[1]Department of Biomedicine, Faculty of Medicine, University of Porto, Porto, Portugal, [2]Chronic Diseases Research Center (CEDOC), Faculty of Medical Sciences, Nova University of Lisbon, Lisbon, Portugal, [3]Center for Neuroscience and Cell Biology (CNC), University of Coimbra, Coimbra, Portugal, [4]Department of Experimental Neurodegeneration, Center for Biostructural Imaging of Neurodegeneration, University Medical Center Göttingen, Göttingen, Germany, [5]Department of Clinical Epidemiology, Predictive Medicine and Public Health, Faculty of Medicine, University of Porto, Porto, Portugal, [6]Department of Public Health Nutrition, Institute of Public Health of the University of Porto (ISPUP), Porto, Portugal, [7]Department of Physiology and Cardiothoracic Surgery, Faculty of Medicine, University of Porto, Porto, Portugal, [8]Faculty of Pharmacy, [9]Faculty of Medicine, University of Coimbra, Coimbra, Portugal, [10]Instituto de Investigação e Inovação em Saúde (i3S), [11]Instituto de Biologia Molecular e Celular (IBMC) and [12]Instituto de Ciências Biomédicas Abel Salazar, University of Porto, Porto, Portugal

*To whom correspondence should be addressed at: Centro de Neurociências e Biologia Celular (CNC), Universidade de Coimbra, Rua Larga, Faculdade de Medicina, Pólo I, 2° andar, 3004-517 Coimbra, Portugal. Tel: +351 913231306; Fax: +351 239822776; Email: pedro.gomes@cnc.uc.pt

Abstract

Insulin resistance is a major predictor of the development of metabolic disorders. Sirtuins (SIRTs) have emerged as potential targets that can be manipulated to counteract age-related diseases, including type 2 diabetes. SIRT2 has been recently shown to exert important metabolic effects, but whether SIRT2 regulates insulin sensitivity in hepatocytes is currently unknown. The aim of this study is to investigate this possibility and to elucidate underlying molecular mechanisms. Here, we show that SIRT2 is downregulated in insulin-resistant hepatocytes and livers, and this was accompanied by increased generation of reactive oxygen species, activation of stress-sensitive ERK1/2 kinase, and mitochondrial dysfunction. Conversely, SIRT2 overexpression in insulin-resistant hepatocytes improved insulin sensitivity, mitigated reactive oxygen species production and ameliorated mitochondrial dysfunction. Further analysis revealed a reestablishment of mitochondrial morphology, with a higher number of elongated mitochondria rather than fragmented mitochondria instigated by insulin resistance. Mechanistically, SIRT2 was able to increase fusion-related protein Mfn2 and decrease mitochondrial-associated Drp1. SIRT2 also attenuated the downregulation of TFAM, a key mtDNA-associated protein, contributing to the increase in mitochondrial mass. Importantly, we found that SIRT2 expression in PBMCs of human subjects was negatively correlated with obesity and

[†]Present address: Laboratory of Metabolic Signaling, Institute of Bioengineering, School of Life Sciences, École Polytechnique Fédérale de Lausanne, CH-1015 Lausanne, Switzerland.

Received: July 19, 2017. **Revised:** July 19, 2017. **Accepted:** July 23, 2017

insulin resistance. These results suggest a novel function for hepatic SIRT2 in the regulation of insulin sensitivity and raise the possibility that SIRT2 activators may offer novel opportunities for preventing or treating insulin resistance and type 2 diabetes.

Introduction

Insulin resistance is a pathophysiological hallmark of metabolic disorders, including obesity and type 2 diabetes, whose incidence has risen to epidemic proportions globally. In the liver, insulin resistance results from the inability of insulin to stimulate hepatic glycogen synthesis and to suppress hepatic glucose production, thus leading to both fasting and postprandial hyperglycemia (1). Despite extensive research, the mechanisms underlying insulin resistance remain incompletely understood (2). It is now recognized that oxidative stress and mitochondrial dysfunction are important contributors to obesity-induced insulin resistance (3–5). Alleviating insulin resistance is still one of the key therapeutic avenues currently available for type 2 diabetes.

Mammalian sirtuins are a conserved family of proteins (SIRT1-7) with NAD^+-dependent deacetylase and/or ADP ribosyltransferase activities, linking their enzymatic activity to the energy state of the organism. Sirtuins are implicated in a myriad of biological processes, including lifespan regulation, metabolism and stress response pathways (6–8). Manipulating their activity may positively impact upon metabolic and age-related disorders (9).

SIRT2 is localized mainly in the cytosol, but can transiently shuttle to the nucleus during mitosis (10). To date, SIRT2 has been ascribed crucial roles in cell cycle regulation (11,12), neurodegeneration (13,14), tumor suppression (12,15) and inflammation (16,17). Accumulating evidence suggests that SIRT2 is an important element on cellular metabolic regulation (18); however, a link between SIRT2 and hepatic insulin resistance has not yet been established. Interestingly, SIRT2 is the most abundant sirtuin in mouse adipose tissue (19), where it is induced by calorie restriction (20,21). Conversely, SIRT2 is downregulated in visceral adipose tissue from human obese subjects (22). SIRT2 also regulates adipocyte differentiation (19,23), sterol and fatty acid biosynthesis (14) and energy expenditure (22). Furthermore, there is evidence suggesting that SIRT2 is able to mitigate oxidative stress and inflammation by deacetylating the redox-sensitive transcription factors forkhead box class O (FOXO) (21) and nuclear factor-κB (NF-κB) (17,24), conditions intimately intertwined with insulin resistance (3–5,25). Importantly, recent studies have shown that SIRT2 interacts with and regulates Akt activation in insulin-responsive cells (26,27).

Based on these premises, we hypothesized that SIRT2 activation may restore metabolic homeostasis and improve insulin sensitivity. Thus, the present study sought to provide evidence that SIRT2 is involved in the regulation of insulin sensitivity in hepatocytes. We find that SIRT2 is downregulated in both insulin-resistant hepatocytes and livers as well as in blood cells from obese and insulin-resistant human subjects, and this is mechanistically linked to high levels of oxidative stress, mitochondrial dysfunction, decreased mitochondrial mass and fragmented mitochondrial network, supporting a derangement in mitochondrial dynamics. Interestingly, we observe that SIRT2 overexpression in hepatocytes improves insulin sensitivity, attenuates reactive oxygen species (ROS) production and mitochondrial dysfunction, and ameliorates all mitochondrial changes. Our data uncover SIRT2 as an important regulator of insulin sensitivity in hepatocytes and suggest that SIRT2 activation might be a useful strategy in type 2 diabetes and other insulin-resistant states.

Results

Reduced hepatic SIRT2 expression under insulin-resistant conditions

Given the ubiquitous expression pattern of SIRT2 and its biological importance in several metabolic pathways (18), together with the central role of the liver in controlling glucose and lipid metabolism, we hypothesized that SIRT2 might have a role in hepatic insulin sensitivity. For this purpose, we first studied the leptin-deficient *ob/ob* mouse, a well-characterized genetic model of severe obesity and insulin resistance (28). As expected, *ob/ob* mice were heavier, had higher epididymal adipose tissue and liver masses, and were hyperglycemic and hyperinsulinemic relative to wild-type (WT) control mice (Table 1). In addition, homeostatic model assessment of insulin resistance (HOMA-IR) indexes of *ob/ob* mice were ∼8-fold increased when compared with WT controls (Fig. 1A). Since increased ROS production appears to trigger insulin resistance in several contexts (5,29), we thus quantified hydrogen peroxide (H_2O_2) levels in WT and insulin-resistant mice. In livers of *ob/ob* mice, H_2O_2 production was significantly higher in comparison with control mice, indicating an increase in oxidative stress (Fig. 1B). There is evidence that oxidative stress-induced MAPK activation plays a significant role in the development of insulin resistance (30). Accordingly, we observed an increase in the phosphorylation state of extracellular signal-regulated kinase (ERK) 1/2 in livers of *ob/ob* mice as compared with control mice (Fig. 1C). We then assessed SIRT2 protein expression in livers of *ob/ob* mice and control mice. SIRT2 can be synthesized in two different forms as the result of alternative splicing (31). Protein levels of SIRT2 long isoform were significantly reduced in livers of *ob/ob* mice as compared with the control group, whereas the short isoform was not altered (Fig. 1D). To determine whether these findings are also observed in a mouse model of high fat diet (HFD)-induced obesity and insulin resistance, we evaluated gene expression patterns in an existing liver tissue dataset (32). Transcriptomic analysis in livers of these mice showed decreased levels of SIRT2 while some genes involved in lipid metabolism and markers of fibrosis and inflammation exhibited opposite trend, such as *Col3a1*, *Ccl2*, *Ccr2* and *Pparg* (Fig. 1E). To experimentally corroborate these genomics derived data, we examined mice fed a HFD for 21 weeks. Due to excessive energy intake, these mice exhibited higher body weight (CD: 31.4 ± 0.9 g versus HFD: 41.2 ± 2.1 g) that was accompanied by higher fasting glucose levels, a standard indicative of insulin resistance (Fig. 1F). Parallel to what was observed in *ob/ob* mice, HFD-fed mice displayed lower levels of SIRT2 (Fig. 1G). Taken together, these results suggest a link between insulin resistance and diminished levels of SIRT2 expression.

We next investigated whether SIRT2 expression is also decreased in a cellular model of insulin resistance. Consistent with previous work (33,34), treatment with glucosamine (GlcN) at a nontoxic concentration for 24 h suppressed insulin-stimulated glycogen synthesis in HepG2 cells (Fig. 2A). Interestingly, the

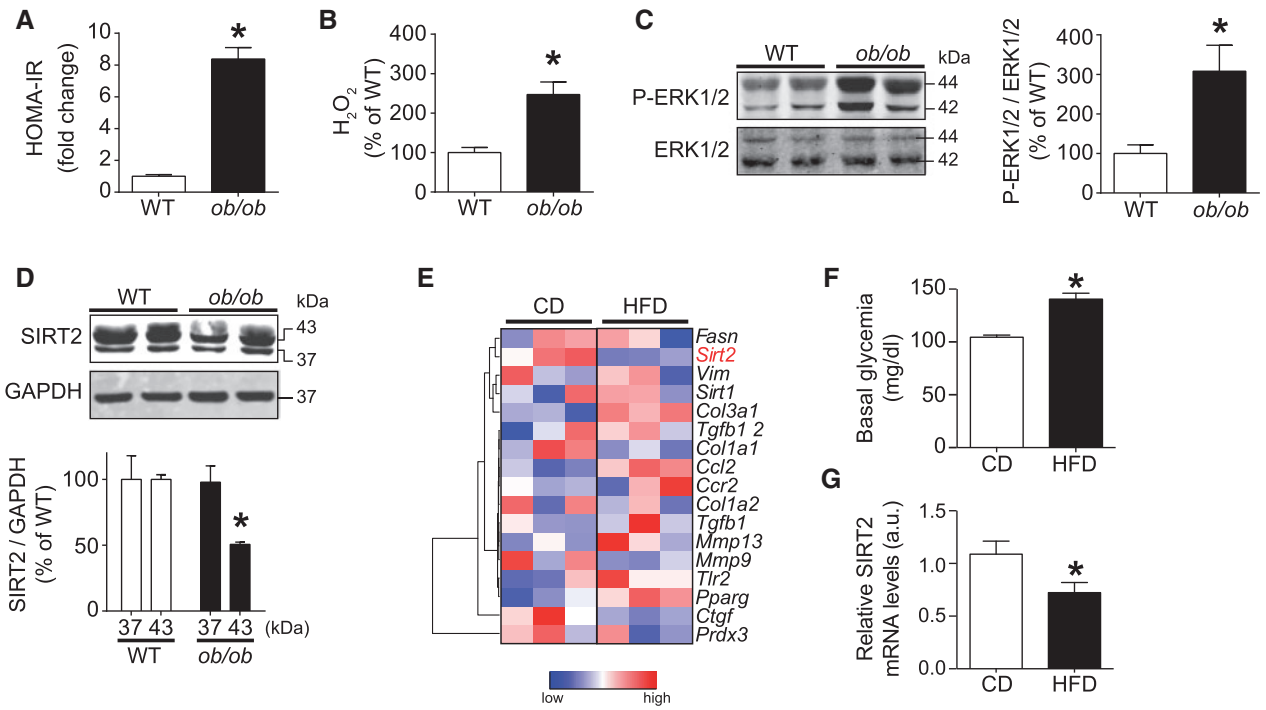

Figure 1. Obese insulin resistant mice exhibit reduced levels of SIRT2 in the liver. (**A**) Insulin resistance as estimated by homeostatic model assessment of insulin resistance (HOMA-IR) in wild-type (WT) and *ob/ob* mice. (**B**) H_2O_2 release from liver tissue of WT and *ob/ob* mice detected using Amplex Red and normalized to the sample protein content. (**C**) Representative western blots showing phosphorylated ERK1/2 (P-ERK1/2) assessed in livers of WT and *ob/ob* mice. Immunoblot of total ERK1/2 served as the loading control. Lower panel shows densitometric analysis of P-ERK1/2 normalized to ERK1/2. (**D**) Representative western blots showing SIRT2 expression in livers of WT and *ob/ob* mice. Two bands were observed, corresponding to the long (43 kDa) and short (39 kDa) isoforms of the SIRT2 proteins. GAPDH used as a loading control. Lower panel shows densitometric analysis of SIRT2 bands normalized to GAPDH. (**E**) Heatmap displaying the relative expression of SIRT2 as well as markers of fibrosis, inflammation and lipid metabolism-related genes in mice fed a high-fat diet (HFD) (32). (**F**) Fasting blood glucose levels in mice fed a standard chow diet (CD) or a high-fat diet (HFD) for 21 weeks. (G) SIRT2 mRNA expression in livers of mice fed a CD or a HFD. Values are expressed as mean ± SEM ($n = 4$–6 for each group; $^*P < 0.05$, comparing the indicated groups).

Table 1. Anthropometric and metabolic parameters of wild-type and *ob/ob* mice

Parameter	Wild-type	*ob/ob*	P-value
Body weight (g)	18.6±1.9	43.1±3.0	<0.001
EpiWAT weight (g)	0.16±0.05	1.55±0.26	<0.001
Liver weight (g)	0.93±0.08	2.81±0.42	<0.001
Glucose (mg/dl)	162.7±6.7	350.2±24.8	<0.001
Insulin (ng/ml)	1.63±0.13	6.43±0.71	<0.001

Data are expressed as mean ± SEM. EpiWAT, epididymal white adipose tissue.

defect in insulin action could be rescued by pioglitazone, a member of the thiazolidinedione class of insulin-sensitizing drugs, lending physiological relevance to this model (Fig. 2A). Pretreatment with N-acetylcysteine (35), a ROS scavenger, reversed GlcN-induced impairment of insulin-induced glycogen synthesis (Fig. 2A), suggesting that oxidative stress underlies insulin resistance in HepG2 cells. Whereas chronic ROS production may contribute to the development of insulin resistance, increasing evidence suggests that transient ROS generation in response to insulin may be required for normal cellular signal transduction (36). Therefore, we examined whether insulin-induced ROS levels and subsequent ERK1/2 signaling were altered in insulin-resistant cells. We found that the transient increase in H_2O_2 levels in control cells in response to insulin (Fig. 2B) coincided with elevated ERK1/2 phosphorylation (Fig. 2C), consistent with ROS participating in normal insulin action. Interestingly, 30-min post-treatment with insulin H_2O_2 levels returned to basal (Fig. 2C). Similar to insulin-resistant mice, GlcN-treated cells exhibited higher basal levels of H_2O_2 (Fig. 2B), which correlated with ERK1/2 hyperphosphorylation (Fig. 2C). Under these conditions, insulin caused an exacerbation in H_2O_2 production (Fig. 2B), but failed to enhance ERK1/2 activation (Fig. 2C). In line with our *in vivo* results, we found a reduction in the expression of both long and short SIRT2 isoforms in insulin-resistant HepG2 cells (Fig. 2D). Collectively, our *in vivo* and *in vitro* observations suggest that hepatic SIRT2 expression is reduced in insulin resistant conditions, possibly by a mechanism involving exaggerated ROS production and consequent ERK1/2 phosphorylation.

SIRT2 overexpression restores insulin sensitivity in insulin-resistant HepG2 cells by counteracting oxidative stress and mitochondrial dysfunction

The reduction of SIRT2 expression under insulin-resistant conditions led us to hypothesize that increasing the dosage of SIRT2 may improve insulin sensitivity. To test this hypothesis, we investigated the effect of SIRT2 overexpression on insulin-stimulated glycogen synthesis and Akt phosphorylation. HepG2 cells were transfected with either wild-type SIRT2 (SIRT2-WT) or a catalytically-inactive mutant (SIRT2-CI) (Fig. 3A). Under normal conditions, overexpressing either SIRT2-WT or SIRT2-CI did not alter insulin-stimulated glycogen synthesis (Fig. 3B) or Akt

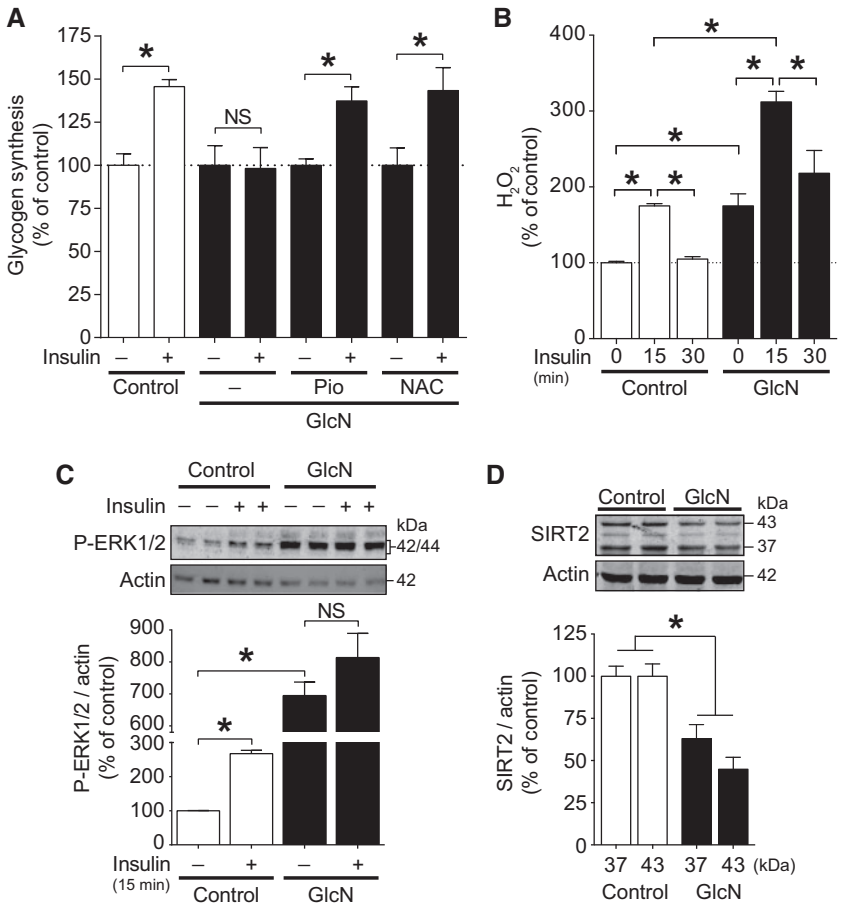

Figure 2. GlcN-induced insulin resistance in HepG2 hepatocytes results in enhanced insulin-stimulated ROS production and decreased SIRT2 protein levels. (**A**) Insulin-stimulated glycogen synthesis. Human HepG2 hepatocytes were pretreated with vehicle (Control) or GlcN (20 mM; 24 h) and then were left unstimulated or stimulated with insulin (100 nM). Where indicated, pioglitazone (Pio) or N-acetylcysteine (NAC) were added simultaneously with GlcN. After 3 h, the cells were harvested and glycogen was quantified as described in Materials and Methods. Values were normalized to the respective basal glycogen synthesis. (**B**) Insulin-stimulated H_2O_2 production. HepG2 cells were pretreated with vehicle (Control) or GlcN (20 mM; 24 h) and then stimulated with insulin (100 nM) for the indicated time. Extracellular levels of H_2O_2 were determined in culture supernatants after incubation with Amplex red. (**C**) Representative western blots showing phosphorylated ERK1/2 (P-ERK1/2) in HepG2 cells pretreated with vehicle or GlcN (20 mM; 24 h) before stimulation with insulin (100 nM; 15 min). Lower panel shows densitometric analysis of P-ERK1/2 normalized to actin. (**D**) Immunoblots showing SIRT2 levels in HepG2 cells treated with vehicle control or GlcN (20 mM; 24 h). Signals were quantified by densitometry and normalized to actin. Values are expressed as mean ± SEM ($n = 3$–6 for each group; *$P < 0.05$, comparing the indicated groups; NS, not significant).

phosphorylation (Fig. 3C). However, under GlcN-induced insulin-resistant conditions, overexpression of SIRT2-WT, but not SIRT2-CI, significantly enhanced insulin-stimulated glycogen synthesis (Fig. 3B) and Akt phosphorylation, although this latter parameter was only partially rescued (Fig. 3C). Overall, these data indicate that increased expression of SIRT2 improves insulin sensitivity under conditions of insulin resistance.

As oxidative stress and mitochondrial dysfunction have been implicated in the etiology of insulin resistance (3–5), we next tested whether upregulating SIRT2 expression affects ROS production and mitochondrial oxygen consumption. Under normal conditions, overexpression of either SIRT2-WT or SIRT2-CI had no effect on H_2O_2 production. Interestingly, under insulin-resistance, enhanced expression of SIRT2-WT resulted in attenuated H_2O_2 levels, whereas no differences were observed upon overexpression of the catalytically inactive SIRT2 (Fig. 4A). Subsequently, we measured the oxygen consumption rate (OCR) in intact HepG2 cells, using a Clark-type oxygen electrode, which enables the evaluation of mitochondrial bioenergetics under conditions that are more physiologically relevant as compared to isolated mitochondria (37). We monitored the OCR in the basal state and after the sequential addition of the ATPase inhibitor oligomycin and the uncoupler FCCP, which stimulates maximal mitochondrial respiration by dissipating the mitochondrial membrane potential (Fig. 4B). No statistically significant differences in the level of basal respiration were observed between control and SIRT2-overexpressing cells; in order to allow direct comparison of bioenergetic profiles between different test conditions we therefore represent changes in respiration relative to normalized basal OCR (Fig. 4C and D). Oligomycin decreased OCR to the same level in either SIRT2-WT or SIRT2-CI cells under both experimental conditions, indicating that there was no difference in non-coupled respiration. However, maximal OCR (after FCCP addition) and spare respiratory capacity (SRC), a measure of mitochondrial fitness (37), were significantly impaired in insulin-resistant cells (Fig. 4C–E), consistent with SIRT2 deficiency causing profound respiratory defects. Importantly, overexpression of SIRT2-WT, but not the deacetylase mutant, restored the ability of mitochondria to reach maximal respiratory capacity and SRC under insulin-resistant conditions (Fig. 4D and E). Moreover, under normal conditions, SIRT2 improved mitochondrial respiration (Fig. 4C and E). Taken

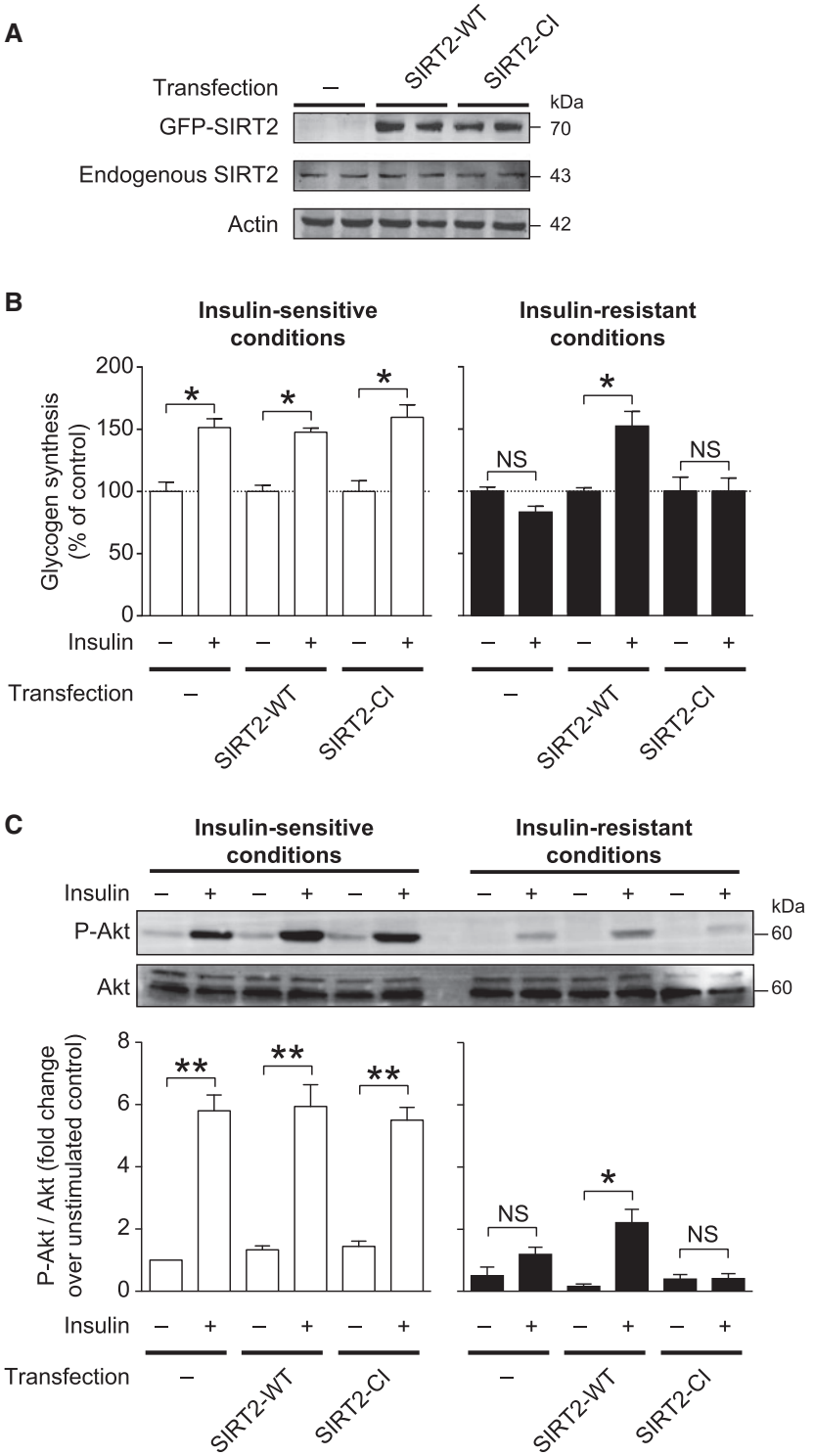

Figure 3. Increased expression of wild-type SIRT2, but not a deacetylase mutant, restores insulin sensitivity in GlcN-treated cells. (**A**) HepG2 cells were transfected with expression plasmids encoding GFP-tagged wild-type SIRT2 (SIRT2-WT) or a catalytically inactive mutant (SIRT2-CI). At 48 h post-transfection, cells were lysed and subjected to western blotting using anti-GFP, anti-SIRT2 and anti-actin. Actin was used as loading control. (**B**) Insulin-stimulated glycogen synthesis. Cells were transfected with the indicated plasmids and after 24 h cells were treated with vehicle (left panel) or GlcN (20 mM; 24 h, right panel) and then were left unstimulated or stimulated with insulin (100 nM; 3h). Glycogen synthesis was subsequently assessed. (**C**) Insulin-stimulated Akt phosphorylation. Representative western blot of basal and insulin-stimulated (100 nM; 15 min) Akt phosphorylation in HepG2 cells under the same conditions as in (**B**). Lower panels show densitometric analysis of P-Akt normalized to total Akt. Values are expressed as mean ± SEM ($n = 3$–6 for each group; $^*P < 0.05$, $^{**}P < 0.01$ comparing the indicated groups; NS, not significant).

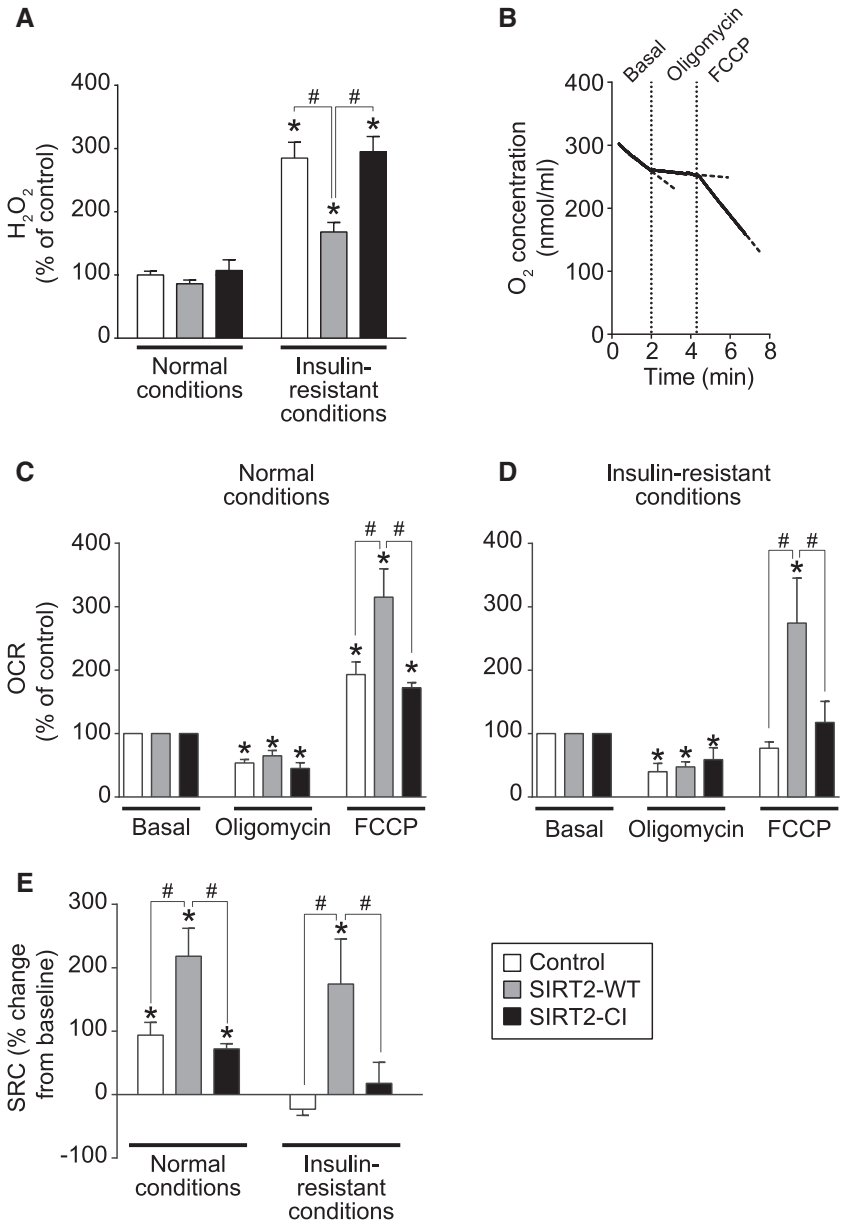

Figure 4. SIRT2 overexpression attenuates ROS generation and improves mitochondrial oxygen consumption associated with insulin-resistant conditions. (**A**) Extracellular H_2O_2 levels in HepG2 cells were determined 48 h post-transfection with the indicated plasmids. At 24 h post-transfection, cells were treated with either vehicle or GlcN (20 mM; 24 h). (**B**) Sample trace demonstrating protocol followed for oxygen consumption measurements in intact HepG2 cells under basal conditions and following the sequential addition of the mitochondrial inhibitor oligomycin (1 μg/ml) and the uncoupler FCCP (1 μM). Dashed lines represent extensions of oxygen consumption rates before indicated additions to more clearly illustrate rate changes. (**C, D**) Oxygen consumption rates (OCR) relative to basal in HepG2 cells were determined under the experimental conditions described in panel A. The differences in OCR are derived from the calculated slope of oxygen utilization and normalized by cell numbers in all assays. (**E**) Spare respiratory capacity (SRC) was calculated from data in panels C and D, as the difference between maximal FCCP-induced respiration and basal respiration. Values are expressed as mean ± SEM ($n = 3$-6 for each group; $^{*}P < 0.05$, compared with corresponding basal values; $^{\S}P < 0.05$, compared with corresponding values under insulin-sensitive conditions; $^{\#}P < 0.05$, comparing the indicated groups).

together, these data indicate that SIRT2 attenuates ROS generation and mitochondrial dysfunction and improves insulin sensitivity in hepatocytes.

SIRT2 deacetylase activity regulates TFAM-dependent mitochondrial biogenesis and mitochondrial morphology in insulin-resistant HepG2 cells

Considering the importance of mitochondrial dynamics to the pathogenesis of insulin resistance (38,39), we therefore hypothesized that SIRT2 could have a role in mitochondrial biogenesis and dynamics, thus justifying the improvement in OCR measurements (Fig. 4C–E). Because a recent study reported that SIRT2 localizes to the inner mitochondrial membrane in central nervous system cells (40), we decided to evaluate the presence of SIRT2 in cytosolic and mitochondrial-enriched fractions of HepG2 cells. Although decreased levels of SIRT2 in GlcN-treated cytosolic extracts reinforced the previous results (Fig. 2D), we were not able to observe SIRT2 in the mitochondria (Fig. 5A). Afterwards, HepG2 cells were co-transfected with SIRT2-WT or

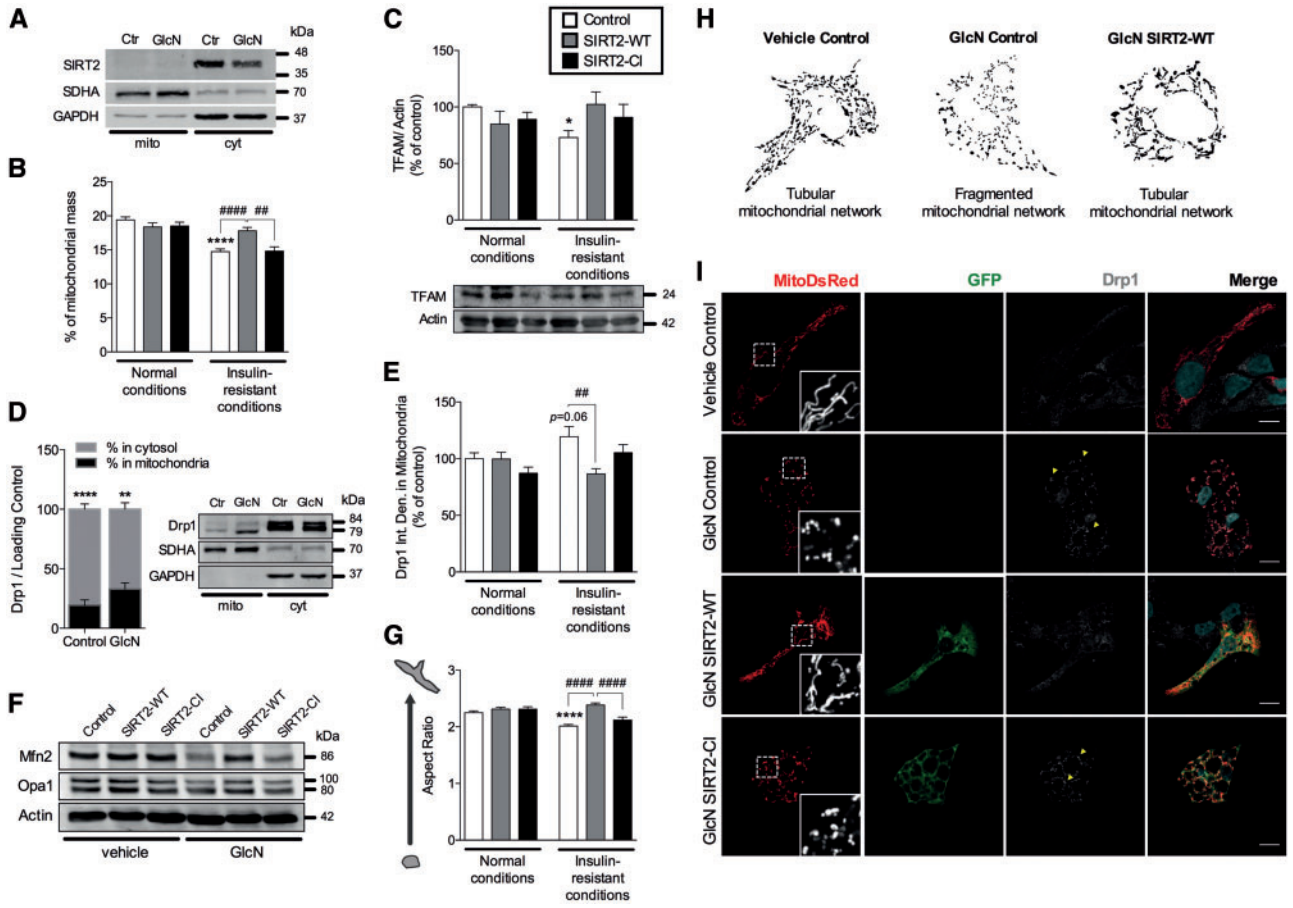

Figure 5. SIRT2 overexpression reestablishes mitochondrial mass and network in insulin-resistant HepG2 hepatocytes. (**A**) Immunoblots showing SIRT2 levels in mitochondrial (mito) and cytosolic (cyt) fractions of HepG2 cells pretreated with vehicle or GlcN (20 mM; 24 h). (**B**) The percentage of cellular area occupied by mitochondria in HepG2 cells was determined 48 h after co-transfection with mitochondrial-targeted DsRed and SIRT2 (WT or CI); nuclei were stained with Hoechst. At 24 h post-transfection, cells were treated with either vehicle or GlcN (20 mM; 24 h). (**C**) Under the same conditions, TFAM levels were detected by western blotting and normalized for actin. Mitochondrial fission factor Drp1 was quantified in (**D**) cyt- and mito-enriched fractions by western blotting of HepG2 cells pretreated with vehicle or GlcN (20 mM; 24 h) and (**E**) its co-localization with mitochondria (yellow arrows) was subsequently determined by immunocytochemistry. (**F**) Representative immunoblots of fusion related proteins Mfn2 and Opa1. Actin was used as loading control. (**G**) Aspect ratio of individual mitochondrion was calculated for each condition using MitoDsRed-transfected HepG2 cells to visualize their mitochondrial network. (**H**) Representative illustrations of fragmented mitochondria, mainly small, round and numerous, and tubular mitochondria, with highly connected network. (**I**) Representative confocal images of HepG2 MitoDsRed/SIRT2-WT/CI co-transfected cells. Scale bar: 10 μm. Images were quantified in ImageJ considering ~20 cells/condition/n. Values are expressed as mean ± SEM ($n = 3$–4 for each group; $^{*}P < 0.05$, $^{****}P < 0.0001$ compared with corresponding basal values; $^{\#\#}P < 0.01$, $^{\#\#\#\#}P < 0.0001$, comparing the indicated groups).

SIRT2-CI plasmids in combination with MitoDsRed to label mitochondrial network. We observed reduced mitochondrial content under GlcN-induced insulin resistant conditions, sustained by a significant decrease in the protein levels of mitochondrial transcription factor A (TFAM) (Fig. 5B and C). Under normal conditions, SIRT2 overexpression had no effect on mitochondrial content. In turn, SIRT2-WT completely recovered the percentage of area occupied by mitochondria in GlcN-treated hepatocytes to the levels of vehicle-treated cells, whereas catalytic inactive SIRT2 was unable to increase the percentage of mitochondrial mass (Fig. 5B). These results suggest that, although SIRT2 does not seem to be present in the mitochondria, its deacetylase activity is required to modulate TFAM-dependent mitochondrial biogenesis.

According to the concept of unbalanced mitochondrial dynamics in insulin resistant conditions (41), we observed a substantial alteration in proteins participating in mitochondrial fission and fusion after GlcN treatment. Under these conditions, the dynamin-related protein 1 (Drp1), a large GTPase primarily found in the cytosol, was shown to be enriched in the mitochondrial fraction (Fig. 5D) where it triggers mitochondrial fragmentation and eventually leads to mitochondria depolarization. Similarly, immunocytochemistry analysis revealed increased Drp1 co-localization with mitochondria in GlcN-treated HepG2 cells (yellow arrows), in contrast to the more diffuse and homogeneous labeling in vehicle conditions (Fig. 5E and I). In addition, mitochondrial fusion-related protein mitofusin 2 (Mfn2) showed decreased protein levels, although no significant changes were observed in optic atrophy 1 (Opa1) (Fig. 5F). Under normal conditions, SIRT2 overexpression did not alter either Drp1 co-localization with mitochondria or fusion protein levels; however, under insulin resistant conditions SIRT2-WT significantly decreased Drp1 in mitochondria and enhanced Mfn2 levels, which was not observed with SIRT2-CI overexpression (Fig. 5E, F and I). The decrease in the translocation of Drp1 to mitochondria, combined with increased Mfn2 expression in the outer mitochondrial membrane induced by SIRT2-WT overexpression ultimately led to an improvement of mitochondrial morphology. While GlcN-treated HepG2 cells displayed a dominant fragmented mitochondrial phenotype, represented

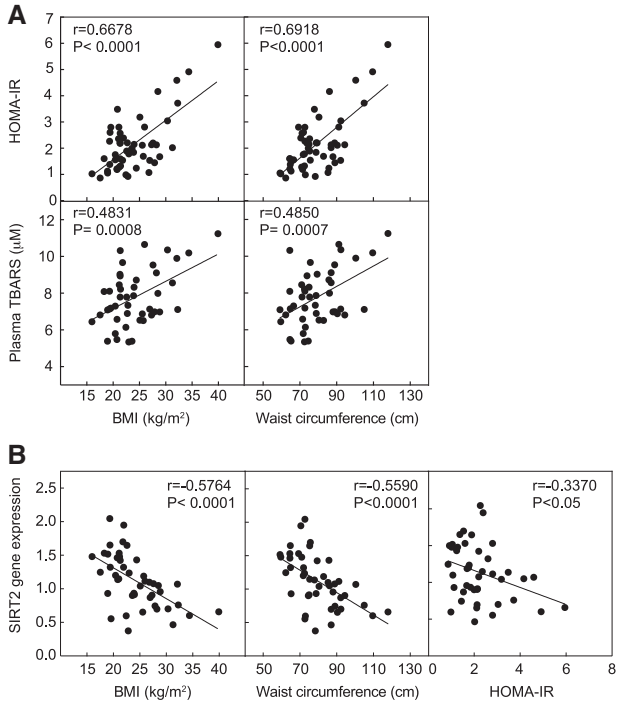

Figure 6. SIRT2 mRNA levels inversely correlate with obesity and insulin resistance in humans. (**A**) Correlation of HOMA-IR and plasma TBARS with obesity indexes (BMI and waist circumference). (**B**) Correlation between SIRT2 transcript levels with obesity (BMI and waist circumference) and insulin resistance (HOMA-IR) indexes in PBMCs from nondiabetic human subjects. Pearson's correlation coefficient (r) is shown for each relationship. HOMA-IR, homeostatic model assessment of insulin resistance; TBARS, thiobarbituric acid reactive substances; PBMCs, peripheral blood mononuclear cells.

Table 2. Anthropometric and metabolic parameters of human subjects according to BMI category

Parameter	BMI < 25 ($n = 27$)	BMI > 25 ($n = 18$)	*P*-value
Gender (M/F)[a]	10/17	8/10	0.852
Age (years)	21.5 ± 0.6	22.2 ± 1.8	0.567
BMI (kg/m^2)	21.0 ± 2.1	29.2 ± 3.7	<0.001
Waist (cm)	71.4 ± 6.5	92.7 ± 9.7	<0.001
% fat	16.4 ± 6.3	31.0 ± 8.6	<0.001
Glucose (mg/dl)	83.2 ± 6.4	86.8 ± 8.6	0.109
Insulin (μU/ml)	8.8 ± 3.1	13.0 ± 6.0	0.015
HOMA-IR	1.8 ± 0.7	2.8 ± 1.4	0.015
Triglycerides (mg/dl)	76.8 ± 26.7	110.1 ± 42.5	0.011
Total cholesterol (mg/dl)	175.0 ± 33.8	193.3 ± 31.3	0.044
LDL (mg/dl)	104.7 ± 29.6	116.8 ± 21.5	0.036
HDL (mg/dl)	55.0 ± 9.0	54.5 ± 18.2	0.286
CRP (mg/l)	0.9 ± 1.7	3.6 ± 3.0	<0.001

Data are expressed as mean ± SD.

[a]Categorical variables were compared using Chi-Square and continuous variables by Mann–Whitney test.

graphically by lower aspect ratio, i.e. the ratio between the major and minor axis of mitochondria that positively correlates with length, SIRT2-WT insulin resistant HepG2 cells presented predominant tubular mitochondrial network with higher aspect ratio (Fig. 5G–I). The recovery of mitochondrial morphology triggered by SIRT2-WT overexpression was not replicated under conditions in which SIRT2 lacks deacetylase activity (Fig. 5G and I). Overall, these findings support that SIRT2 directly favors mitochondrial biogenesis and elongation in an insulin-resistant hepatocyte cell model, which may reciprocally influence bioenergetics.

SIRT2 mRNA levels correlate inversely with obesity and insulin resistance in humans

Finally, we investigated whether SIRT2 deficiency is associated with obesity and insulin resistance in human individuals. Clinical parameters of 45 Caucasian non-diabetic subjects stratified into two groups according to the body mass index (BMI) are presented in Table 2. In addition to a greater BMI, overweight and obese subjects had higher fasting hyperinsulinemia and hypertriglyceridemia. We observed a strong positive correlation between insulin resistance, measured by the HOMA-IR index, and obesity-related traits (BMI and waist circumference) (Fig. 6A). To determine whether oxidative stress is increased in these overweight and obese subjects, we measured lipid peroxidation, a marker of oxidative injury. Lipid peroxidation, represented by plasma thiobarbituric acid reactive substance (TBARS), was positively correlated with BMI and waist circumference (Fig. 6A). Finally, we quantified SIRT2 mRNA expression in PBMCs of the human subjects. Interestingly, SIRT2 mRNA levels were negatively correlated with both indexes of obesity (BMI and waist circumference) and insulin resistance (HOMA-IR) (Fig. 6B). Taken together, these results suggest that SIRT2 downregulation is associated with oxidative stress-related obesity and insulin resistance in humans.

Discussion

The present study provides the first direct evidence that SIRT2 is involved in the regulation of hepatic insulin sensitivity. First, we observed a reduction in SIRT2 expression levels in the livers of both genetic and diet-induced obese and insulin-resistant mice. Second, SIRT2 protein expression was significantly reduced in an insulin-resistant HepG2 cell model. Third, we found that elevated SIRT2 expression improved insulin signaling and enhanced insulin sensitivity in insulin-resistant HepG2 cells. Finally, we found that SIRT2 gene expression in PBMCs from human subjects is inversely correlated with obesity and insulin resistance. Taken together, these data suggest that positive energy balance concomitant with insulin resistance in both rodents and humans suppresses expression and potentially activity of SIRT2.

A growing body of literature supports a role for SIRT2 in the regulation of important metabolic pathways (14,18,19,21–23,42,43). However, available data on the role of SIRT2 in insulin signaling have revealed contradictory findings. Consistent with our results, recent studies showed that SIRT2 interacts with and positively regulates Akt activation in insulin-responsive 3T3-L1 preadipocytes and HeLa cells (26) and in LUHMES neuronal cells (44). While SIRT2 overexpression enhanced insulin-induced Akt activation and phosphorylation of its downstream targets (26), pharmacological or genetic SIRT2 inhibition causes the opposite effect (26,44). In contrast, another study showed increased SIRT2 expression in insulin-resistant C2C12 skeletal muscle cells and that SIRT2 inhibition, by either pharmacological or genetic means, increased insulin-stimulated glucose uptake and improved phosphorylation of Akt and GSK3β under insulin

resistance conditions, suggesting that SIRT2 may negatively affect skeletal muscle glucose uptake (45). The discrepancy between these findings might be explained by differences in the cellular models of insulin resistance. It is possible that SIRT2 in different tissues may play distinctive and even opposing roles with respect to insulin sensitivity. A similar scenario has been previously reported for SIRT1, in which hepatic SIRT1 deficiency leads to insulin resistance (46), whereas neuronal SIRT1 deficiency improves insulin sensitivity in both brain and peripheral tissues (47). Whether SIRT2 displays tissue-specific metabolic actions has yet to be determined, but these studies suggest that possibility.

The improvement in insulin sensitivity by SIRT2 appears to be mediated, at least in part, by its effects on oxidative stress and mitochondrial dysfunction, two conditions intimately associated with insulin resistance (3–5,25). Multiple lines of evidence from our data support this hypothesis. First, we observed increased H_2O_2 levels in both insulin-resistant livers and cells, and increased plasma TBARS, a lipid peroxidation marker, in insulin-resistant humans, and this was associated with decreased SIRT2 mRNA levels. Second, we found that GlcN-induced insulin resistance is associated with mitochondrial dysfunction, as indicated by the inability of HepG2 cells to achieve maximal respiration after addition of FCCP and low spare respiratory capacity, suggesting reduced capacity to produce energy under conditions of increased work or stress (37). Concordantly, in human fibroblasts, reduced levels of SIRT2 caused decreased oxidative phosphorylation and glycolysis activation (48). SIRT2 has been reported to suppress intracellular ROS levels by deacetylating and thus activating FOXO3a-dependent antioxidant defense mechanisms (21). Moreover, the beneficial effect of SIRT2 against oxidative stress and mitochondrial dysfunction seems to be dependent on its catalytic activity, as overexpression of full length SIRT2, but not of a catalytically inactive mutant, attenuated GlcN-induced ROS production (Fig. 4A) and concomitantly restored FCCP-induced maximal respiration (Fig. 4C and D) and spare respiratory capacity (Fig. 4E). Insulin resistance-mediated decreased SIRT2 and modified mitochondrial function appear to be related to unbalanced mitochondrial dynamics and decreased TFAM-dependent mitochondrial biogenesis. Indeed, to maintain their function mitochondria constantly undergo fusion and fission events; simultaneously, novel mitochondrial components are being formed and the organelle is degraded. The disruption of these dynamics may underlie the pathogenesis of insulin resistance in obesity and type 2 diabetes (38,39). Interestingly, we found that SIRT2 could ameliorate the changes in TFAM levels and thus mitochondrial mass. Considering that PGC-1α coactivates nuclear respiratory factors (NRF-1 and NRF-2), which regulate the expression of TFAM, and that $SIRT2^{-/-}$ mice exhibited increased PGC-1a acetylation (40), we may anticipate that reduced TFAM-dependent biogenesis in insulin resistant conditions may be linked to increased acetylation and thus decreased activity of PGC-1α. SIRT2 was also shown to reverse the derangement of mitochondrial dynamics by re-establishing a tubular mitochondrial network, which was mechanistically linked to enhanced levels Mfn2 and decreased Drp1 in mitochondria. Notably, in contrast with Liu *et al.* (40), we did not detect SIRT2 in mitochondrial fractions isolated from hepatocyte cells, implicating that its deacetylase activity might be required to modulate both mitochondrial dynamics and function, possibly by modifying primarily cytosolic proteins, such as Drp1.

Another potential mechanism linking SIRT2 downregulation and insulin resistance is the ERK1/2 pathway. It is widely accepted that insulin can activate both phosphoinositide 3-kinase (PI3K)/Akt pathway, which is responsible for glucose metabolism, and several proteins in the MAPK signaling pathway (c-Jun NH2-terminal kinase [JNK], p38 and ERK1/2), which results in decreased insulin signaling and is crucial for insulin resistance (49). In the current study, we demonstrate that low SIRT2 levels in both insulin-resistant livers and HepG2 cells are associated with exaggerated phosphorylation of ERK1/2 and increased production of ROS, indicating that ERK1/2 activation seems a causal factor for insulin resistance caused by oxidative stress. Accordingly, oxidative stress induces insulin resistance in cardiomyocytes and hearts of diabetic mice, which is associated with ERK overactivation (50). Moreover, ERK inhibition reversed the impaired insulin sensitivity (50). Collectively, our observations suggest that increased ROS levels, ERK1/2 activation and mitochondrial dysfunction together with SIRT2 deficiency, may decrease insulin signaling *in vitro* and *in vivo* to promote the development of insulin resistance.

SIRT2 mRNA and/or protein levels in PBMCs may represent a potential and novel pathogenic marker of insulin resistance in humans. PBMCs are readily accessible biological material and, more importantly, their gene expression is representative of whole metabolic status (51,52). Although the biological regulation of SIRT2 in PBMCs may not parallel that in insulin-responsive tissues, such as the liver, a recent study demonstrated that SIRT2 gene expression in PBMCs of obese subjects was induced by calorie restriction (20). In addition, the surrogate measure of insulin resistance used in this study (HOMA-IR) correlates reasonably well with the insulin clamp (53), and primarily reflects hepatic insulin sensitivity, since the fasting plasma glucose is determined mainly by the rate of hepatic glucose production (HGP) and insulin is the primary regulator of HGP. Although we cannot translate this observation directly to other insulin-sensitive cells, we hypothesize that this relationship may also be true in tissues that play a relevant role in determining insulin resistance.

In conclusion, our work proposes SIRT2 as an important regulator of insulin sensitivity and may represent a novel therapeutic approach for the prevention and/or treatment of insulin resistance and its associated comorbidities.

Materials and Methods

Mice

Experimental procedures complied with the Declaration of Helsinki and have been approved by the Ethics Committee of the University of Porto. Mice were purchased from Charles River and housed in a temperature-controlled (20–22 °C) room on a 12-h light/dark cycle, and chow and water were provided *ad libitum*. Eight-week-old male *ob/ob* mice and their age-matched lean control C57BL/6J mice were anesthetized using sodium pentobarbital (60 mg/kg, i.p.) and blood and liver tissue were collected. Fasting blood glucose and plasma insulin concentrations were used for the estimation of HOMA-IR (54). Eight-week-old C57BL/6J mice were fed either a CD or a HFD (D12492, Research Diets) for 21 weeks. A blood sample was obtained by nicking the lateral tail vein to measure glycemia with a glucometer after overnight fasting.

Cell culture, treatment and transfections

HepG2 human hepatoma cells were obtained from American Type Culture Collection. Cells were maintained in MEM (Sigma) supplemented with 10% heat-inactivated FBS (Gibco) and 1%

penicillin/streptomycin. Cells were maintained at 37 °C under a humidified atmosphere with 5% CO_2. To induce insulin resistance, HepG2 cells were treated with 20 mM glucosamine for 24 h in serum-free MEM. Under these conditions, there was no significant effect on cell viability (data not shown). All transfections consisted in combining Lipofectamine 2000 reagent (Invitrogen) with Opti-MEM followed by the addition of the plasmid of interest. The resulting complexes were then added to the cells and incubated for 48 h.

Measurement of H_2O_2 production

Fresh liver tissue from WT and *ob/ob* mice was cut into square pieces and incubated at 37 °C in Krebs-HEPES buffer (118 mM NaCl, 4.5 mM KCl, 2.5 mM $CaCl_2$, 1.2 mM $MgCl_2$, 1.2 mM K_2HPO_4, 25 mM $NaHCO_3$, 25 mM Na-HEPES, and 5 mM glucose; pH 7.4) for 90 min, with oxygenation and constant shaking, as previously described (29). After incubation, the resulting supernatants were transferred to a 96-well plate and tissues were weighed to normalize final results. HepG2 cells were cultured in 96-well plates, treated and the medium transferred to a replica plate. H_2O_2 released from tissue or cells was then detected using the Amplex Red Hydrogen Peroxide/Peroxidase assay kit (Molecular Probes), following manufacturer's instructions. Fluorescence intensity was measured in a Spectramax Gemini XS microplate reader (Molecular Devices) at an excitation wavelength of 530 nm and emission wavelength of 590 nm, for 40 min at room temperature, following the kinetics of the reaction (every 1 min).

Western blot analysis

For total protein lysates, liver tissue or HepG2 cells were homogenized in ice-cold radioimmunoprecipitation assay (RIPA) buffer (50 mM Tris-HCl pH 7.4, 150 mM NaCl, 1% NP-40, 1 mM EDTA) containing protease and phosphatase inhibitors. For cytosolic and mitochondrial-enriched fractions, HepG2 cells were homogenized with a Potter-Elvejhem 377 homogenizer with a Teflon pestle, at 300 rpm, in ice-cold sucrose buffer (250 mM sucrose, 20 mM HEPES/KOH (pH 7.5), 100 mM KCl, 1.5 mM $MgCl_2$, 1 mM EGTA, 1 mM EDTA), supplemented with protease and phosphatase inhibitors. Resulting lysates were centrifuged at 1, 088 x *g* for 12 min (4 °C) to pellet the nuclei and cell debris. The supernatant was further centrifuged at 12, 000 x *g* for 20 min (4 °C) and the resulting pellet (mitochondrial-enriched fraction) re-suspended in supplemented sucrose buffer. Trichloroacetic acid (15%) was added to the supernatant, and precipitated proteins were centrifuged at 16, 300 × *g* for 10 min (4 °C). The resulting pellet (cytosolic fraction) was re-suspended in supplemented sucrose buffer and brought to pH 7 with KOH. Protein concentrations were quantified using the BCA protein assay kit (Pierce). Equal amounts of total protein (30–50 μg) were separated by 10% SDS-PAGE, transferred to nitrocellulose membranes, and incubated for 1 h with a blocking solution (5% nonfat dry milk, 0.1% Tween-20 in TBS). Immunodetection was performed using anti-P-ERK1/2 (Cell Signaling), anti-ERK1/2 (Cell Signaling), anti-SIRT2 (Sigma Aldrich), anti-GFP (Santa Cruz), anti-TFAM (Abcam), anti-Drp1 (BD Biosciences), anti-Mitofusin 2 (Sigma), anti-Opa1 (BD Biosciences), anti-GAPDH (Santa Cruz) and anti-actin (Santa Cruz) antibodies. A 1: 20, 000 dilution of the appropriate fluorescently labeled secondary antibodies (Rockland) were used to detect the resulting immune complexes. Detection was performed using Odyssey infrared imaging system (LI-COR Biosciences).

Glycogen synthesis

HepG2 cells were seeded at a density of 6×10^4 cells/cm^2 in 24-well culture plates. After 24 h, cells were washed with serum-free MEM and incubated for 24 h with the same medium in the presence or absence of 20 mM glucosamine. The medium was then replaced by 500 μl of MEM containing 1 μCi/ml D-[^{3}H]glucose and incubated in the presence or absence of 100 nM insulin for 3 h. Cells in each well were then lysed in 200 μl of 30% KOH with 5 mg/ml glycogen for 30 min at 60 °C. Cell lysates were transferred to polypropylene tubes, and glycogen was precipitated overnight at −20 °C by adding 1 ml of absolute ethanol. Glycogen was then separated by centrifugation at 5000 × *g* for 10 min, and the pellets washed twice with 75% ice-cold ethanol. Finally, the pellets were solubilized in 200 μl of 0.1 M HCl and measured in a liquid scintillation counter by adding 4 ml of high-flashpoint scintillation cocktail.

Oxygen consumption in intact HepG2 cells

Oxygen consumption was measured with a Clark-type oxygen electrode. Each experimental condition was analyzed by incubating 1.5×10^6 cells in PBS in a magnetically stirred chamber thermostated to 37 °C. After recording basal respiration, uncoupled respiration (proton leak) was measured by adding 2.5 μg/ml of ATP synthase inhibitor oligomycin (Sigma). Subsequently, 1 μM of cyanide *p*-trifluoromethoxyphenylhydrazone (FCCP, Sigma) was added to the chamber to measure maximum respiration. Mitochondrial spare respiratory capacity (SRC) was calculated by subtracting the basal respiration to the maximal respiration (SRC = FCCP-driven respiration – basal respiration).

Immunocytochemistry

HepG2 cells plated in gelatin-coated 16 mm coverslips were washed twice with warm PBS, fixed with 4% paraformaldehyde for 20 min, permeabilized in 0.1% Triton X-100 in PBS for 2 min and blocked for 1 h, at room temperature in 3% (w/v) BSA in PBS. Incubation with anti-Drp1 primary antibody (1: 300, BD biosciences) occurred overnight, at 4 °C. In the following day, cells were incubated for 1 h, at room temperature, with secondary antibody alexa fluor-633 donkey anti-mouse (1: 300, Molecular Probes). All antibodies were prepared in 3% (w/v) BSA in PBS. Finally, cells were incubated with Hoechst 33342 (4 μg/ml) for 20 min and mounted using fluoroshield mounting medium (Abcam).

Image acquisition and analysis

Confocal images were obtained using a Plan-Apochromat/1.4 NA 63x lens on an Axio Observer.Z1 confocal microscope (Zeiss Microscopy, Germany) with Zeiss LSM 710 software. Mitochondria area, morphology and protein co-localization analysis was achieved using Macros for Fiji designed by Dr. Jorge Valero (Achucarro Basque Center for Neuroscience, Spain), in Fiji. Briefly, nonspecific background noise was corrected using the Subtract Background function included in Fiji (rolling ball radius: 10 μm for 8 bit transformed images). For analysis of mitochondrial network HepG2 cells were transfected with cytochrome c oxidase subunit VIII-targeted DsRed (MitoDsRed, Clontech). FindFoci function was used to allow the identification of peak intensity regions and a threshold was applied to optimally create a mitochondrial mask with individualized mitochondria. Mitochondrial network was traced through

Analyze Particles function and Aspect ratio (ratio between the major and minor axis of mitochondria) was used as an index of mitochondrial length. For protein co-localization with mitochondria a threshold was set and the Integrated Density (Int. Den.) measured inside the mitochondrial region of interest. Data were normalized for cellular area.

Human studies

The study protocols were conducted in accordance with the aforementioned institutional guidelines. Subjects ($n = 45$) were selected from the Epidemiological Health Investigation of Teenagers in Porto (EPITeen) cohort and followed at the Department of Clinical Epidemiology, Predictive Medicine and Public Health of the University of Porto. The recruitment and characteristics of the cohort were previously described (55). The nature and potential risks of the study were explained to all subjects before obtaining their written informed consent. Each subject completed a questionnaire to collect history regarding smoking and alcohol consumption, as well as other demographic characteristics, such as age and family history of cancer, diabetes, and cardiovascular disease. Exclusion criteria included regular exercise (>90 min of aerobic activity per week), usage of medications (e.g. antidiabetics) or dietary supplements (e.g. antioxidants), and a known history of disease (i.e. type 2 diabetes, dyslipidemia, or arterial hypertension). Participants were instructed to abstain from smoking and alcohol consumption at least 24 h before the study. Anthropometric measurements including height, weight and waist circumference, were taken according to standardized procedures. Body fat percentage was measured with a bioimpedance analyzer of body composition. For the present analysis, we included subjects with a body mass index (BMI) ranging from 15 to 40 kg/m^2. BMI was calculated as weight (in kilograms) divided by square of height (in meters). Subjects were stratified into two BMI groups: normal ($BMI < 25\ kg/m^2$) and overweight/obese ($BMI > 25\ kg/m^2$).

PBMCs isolation and measurement of biomarkers

After informed consent, participants provided a peripheral blood sample. Plasma and peripheral blood mononuclear cells (PBMCs) were isolated from whole blood by density gradient centrifugation on Histopaque 1077 (Sigma). Plasma samples were analyzed for fasting glucose, insulin, triglycerides, total cholesterol and high-density lipoprotein (HDL) and low-density lipoprotein (LDL). Insulin resistance was evaluated by the HOMA-IR (54). Plasma samples were also analyzed for thiobarbituric acid reactive substances (TBARS), as a marker of lipid peroxidation, using a spectrophotometric method (56).

Total RNA extraction and quantitative real time PCR

Total RNA was extracted from livers of CD- and HFD-fed mice and from PBMCs isolated from human blood samples using Trizol (Invitrogen), according to manufacturer's instructions. cDNAs were produced using first strand cDNA synthesis kit (Fermentas). Quantitative PCR was performed in a StepOne Plus Real Time PCR system (Applied Biosystems) using SIRT2 and actin primers. All PCR reactions were performed in triplicate and amplified using Kapa SYBR Fast Universal qPCR kit (Kapa Biosystems). Relative quantification of SIRT2 gene expression normalized to actin or β-2-microglobulin housekeeping genes was carried out using the comparative CT method. Microarray analysis was performed on published transcriptomics (GEO GSE32095). Heat maps were generated using GENE-E (http://www.broadinstitute.org/cancer/software/GENE-E/index.html), and rows were clustered using the one minus Pearson correlation metric.

Data analysis

Statistical analyses were performed with SPSS Version 19.0. All data are presented as mean ± SEM, except for data in Table 2, which are presented as mean ± SD. Normal distribution was verified with the Kolmogorov-Smirnov test. Differences between two groups were assessed using the Student's unpaired t test or the Mann-Whitney test, for normally and not normally distributed variables, respectively. Comparisons between multiple groups were performed using one-way analysis of variance (ANOVA). Associations among variables were assessed with the use of Pearson's correlation coefficient. Differences were considered statistically significant at $P < 0.05$.

Acknowledgements

We thank Prof. Eric Verdin (University of California, San Francisco) for the generous gift of the SIRT2 plasmids (GFP-SIRT2 and GFP-SIRT2 H187Y).

Conflict of Interest statement. None declared.

Funding

European Regional Development Fund (ERDF), Centro 2020 Regional Operational Programme (CENTRO-01-0145-FEDER-000012: HealthyAging2020); COMPETE 2020 - Operational Programme for Competitiveness and Internationalisation and Portuguese national funds via FCT – Fundação para a Ciência e a Tecnologia (POCI-01-0145-FEDER-007440, SFRH/BPD/109347/2015 to R.M.O., SFRH/BD/86655/2012 to L.N. and SFRH/BPD/111815/2015 to P.G.); FLAD Life Science 2020 Grant to A.C.R.; European Molecular Biology Organization (EMBO Installation Grant to T.F.O.); DFG Center for Nanoscale Microscopy and Molecular Physiology of the Brain (CNMPB) to T.F.O.

References

1. Roden, M. and Bernroider, E. (2003) Hepatic glucose metabolism in humans–its role in health and disease. *Best Pract. Res. Clin. Endocrinol. Metab.*, **17**, 365–383.
2. Qatanani, M. and Lazar, M.A. (2007) Mechanisms of obesity-associated insulin resistance: many choices on the menu. *Genes Dev.*, **21**, 1443–1455.
3. Kim, J.A., Wei, Y. and Sowers, J.R. (2008) Role of mitochondrial dysfunction in insulin resistance. *Circ. Res.*, **102**, 401–414.
4. Meigs, J.B., Larson, M.G., Fox, C.S., Keaney, J.F., Jr., Vasan, R.S. and Benjamin, E.J. (2007) Association of oxidative stress, insulin resistance, and diabetes risk phenotypes: the Framingham Offspring Study. *Diabetes Care*, **30**, 2529–2535.
5. Houstis, N., Rosen, E.D. and Lander, E.S. (2006) Reactive oxygen species have a causal role in multiple forms of insulin resistance. *Nature*, **440**, 944–948.
6. Donmez, G. and Guarente, L. (2010) Aging and disease: connections to sirtuins. *Aging Cell*, **9**, 285–290.

7. Haigis, M.C. and Sinclair, D.A. (2010) Mammalian sirtuins: biological insights and disease relevance. *Annu. Rev. Pathol.*, **5**, 253–295.
8. Chalkiadaki, A. and Guarente, L. (2012) Sirtuins mediate mammalian metabolic responses to nutrient availability. *Nat. Rev. Endocrinol.*, **8**, 287–296.
9. Baur, J.A., Ungvari, Z., Minor, R.K., Le Couteur, D.G. and de Cabo, R. (2012) Are sirtuins viable targets for improving healthspan and lifespan? *Nat. Rev. Drug Discov.*, **11**, 443–461.
10. North, B.J. and Verdin, E. (2007) Interphase nucleo-cytoplasmic shuttling and localization of SIRT2 during mitosis. *Plos One*, **2**, e784.
11. Dryden, S.C., Nahhas, F.A., Nowak, J.E., Goustin, A.S. and Tainsky, M.A. (2003) Role for human SIRT2 NAD-dependent deacetylase activity in control of mitotic exit in the cell cycle. *Mol. Cell. Biol.*, **23**, 3173–3185.
12. Serrano, L., Martinez-Redondo, P., Marazuela-Duque, A., Vazquez, B.N., Dooley, S.J., Voigt, P., Beck, D.B., Kane-Goldsmith, N., Tong, Q. and Rabanal, R.M. (2013) The tumor suppressor SirT2 regulates cell cycle progression and genome stability by modulating the mitotic deposition of H4K20 methylation. *Genes Dev.*, **27**, 639–653.
13. Outeiro, T.F., Kontopoulos, E., Altmann, S.M., Kufareva, I., Strathearn, K.E., Amore, A.M., Volk, C.B., Maxwell, M.M., Rochet, J.C. and McLean, P.J. (2007) Sirtuin 2 inhibitors rescue alpha-synuclein-mediated toxicity in models of Parkinson's disease. *Science*, **317**, 516–519.
14. Luthi-Carter, R., Taylor, D.M., Pallos, J., Lambert, E., Amore, A., Parker, A., Moffitt, H., Smith, D.L., Runne, H., Gokce, O. *et al.* (2010) SIRT2 inhibition achieves neuroprotection by decreasing sterol biosynthesis. *Proc. Natl Acad. Sci. USA*, **107**, 7927–7932.
15. Kim, H.S., Vassilopoulos, A., Wang, R.H., Lahusen, T., Xiao, Z., Xu, X., Li, C., Veenstra, T.D., Li, B., Yu, H. *et al.* (2011) SIRT2 maintains genome integrity and suppresses tumorigenesis through regulating APC/C activity. *Cancer Cell*, **20**, 487–499.
16. Lin, J., Sun, B., Jiang, C., Hong, H. and Zheng, Y. (2013) Sirt2 suppresses inflammatory responses in collagen-induced arthritis. *Biochem. Biophys. Res. Commun.*, **441**, 897–903.
17. Pais, T.F., Szegő, É.M., Marques, O., Miller-Fleming, L., Antas, P., Guerreiro, P., de Oliveira, R.M., Kasapoglu, B. and Outeiro, T.F. (2013) The NAD-dependent deacetylase sirtuin 2 is a suppressor of microglial activation and brain inflammation. *EMBO J.*, **32**, 2603–2616.
18. Gomes, P., Outeiro, T.F. and Cavadas, C. (2015) Emerging role of sirtuin 2 in the regulation of mammalian metabolism. *Trends Pharmacol. Sci.*, **36**, 756–768.
19. Jing, E., Gesta, S. and Kahn, C.R. (2007) SIRT2 regulates adipocyte differentiation through FoxO1 acetylation/deacetylation. *Cell Metab.*, **6**, 105–114.
20. Crujeiras, A.B., Parra, D., Goyenechea, E. and Martinez, J.A. (2008) Sirtuin gene expression in human mononuclear cells is modulated by caloric restriction. *Eur. J. Clin. Invest.*, **38**, 672–678.
21. Wang, F., Nguyen, M., Qin, F.X. and Tong, Q. (2007) SIRT2 deacetylates FOXO3a in response to oxidative stress and caloric restriction. *Aging Cell*, **6**, 505–514.
22. Krishnan, J., Danzer, C., Simka, T., Ukropec, J., Walter, K.M., Kumpf, S., Mirtschink, P., Ukropcova, B., Gasperikova, D., Pedrazzini, T. and Krek, W. (2012) Dietary obesity-associated Hif1alpha activation in adipocytes restricts fatty acid oxidation and energy expenditure via suppression of the Sirt2-NAD+ system. *Genes Dev.*, **26**, 259–270.
23. Wang, F. and Tong, Q. (2009) SIRT2 suppresses adipocyte differentiation by deacetylating FOXO1 and enhancing FOXO1's repressive interaction with PPARg. *Mol. Biol. Cell*, **20**, 801–808.
24. Rothgiesser, K.M., Erener, S., Waibel, S., Lüscher, B. and Hottiger, M.O. (2010) SIRT2 regulates NF-kB-dependent gene expression through deacetylation of p65 Lys310. *J. Cell Sci.*, **123**, 4251–4258.
25. Kim, J.K. (2012) Endothelial NF-kB in obesity and aging: is endothelial NF-kB a master regulator of inflammation and insulin resistance? *Circulation*, **125**, 1081–1083.
26. Ramakrishnan, G., Davaakhuu, G., Kaplun, L., Chung, W.C., Rana, A., Atfi, A., Miele, L. and Tzivion, G. (2014) Sirt2 deacetylase is a novel AKT binding partner critical for AKT activation by insulin. *J. Biol. Chem.*, **289**, 6054–6066.
27. Chen, J., Chan, A.W.H., To, K.-F., Chen, W., Zhang, Z., Ren, J., Song, C., Cheung, Y.-S., Lai, P.B.S., Cheng, S.-H. *et al.* (2013) SIRT2 overexpression in hepatocellular carcinoma mediates epithelial to mesenchymal transition by protein kinase B/glycogen synthase kinase-3beta/beta-catenin signaling. *Hepatology*, **57**, 2287–2298.
28. Kennedy, A.J., Ellacott, K.L., King, V.L. and Hasty, A.H. (2010) Mouse models of the metabolic syndrome. *Dis. Model. Mech.*, **3**, 156–166.
29. Furukawa, S., Fujita, T., Shimabukuro, M., Iwaki, M., Yamada, Y., Nakajima, Y., Nakayama, O., Makishima, M., Matsuda, M. and Shimomura, I. (2004) Increased oxidative stress in obesity and its impact on metabolic syndrome. *J. Clin. Invest.*, **114**, 1752–1761.
30. Evans, J.L., Goldfine, I.D., Maddux, B.A. and Grodsky, G.M. (2003) Are oxidative stress-activated signaling pathways mediators of insulin resistance and beta-cell dysfunction? *Diabetes*, **52**, 1–8.
31. Voelter-Mahlknecht, S., Ho, A.D. and Mahlknecht, U. (2005) FISH-mapping and genomic organization of the NAD-dependent histone deacetylase gene, Sirtuin 2 (Sirt2). *Int. J. Oncol.*, **27**, 1187–1196.
32. Ichimura, A., Hirasawa, A., Poulain-Godefroy, O., Bonnefond, A., Hara, T., Yengo, L., Kimura, I., Leloire, A., Liu, N., Iida, K. *et al.* (2012) Dysfunction of lipid sensor GPR120 leads to obesity in both mouse and human. *Nature*, **483**, 350–354.
33. Sun, C., Zhang, F., Ge, X., Yan, T., Chen, X., Shi, X. and Zhai, Q. (2007) SIRT1 improves insulin sensitivity under insulin-resistant conditions by repressing PTP1B. *Cell Metab.*, **6**, 307–319.
34. Zhou, B., Li, C., Qi, W., Zhang, Y., Zhang, F., Wu, J.X., Hu, Y.N., Wu, D.M., Liu, Y., Yan, T.T. *et al.* (2012) Downregulation of miR-181a upregulates sirtuin-1 (SIRT1) and improves hepatic insulin sensitivity. *Diabetologia*, **55**, 2032–2043.
35. Milanski, M., Arruda, A.P., Coope, A., Ignacio-Souza, L.M., Nunez, C.E., Roman, E.A., Romanatto, T., Pascoal, L.B., Caricilli, A.M., Torsoni, M.A. *et al.* (2012) Inhibition of hypothalamic inflammation reverses diet-induced insulin resistance in the liver. *Diabetes*, **61**, 1455–1462.
36. Bashan, N., Kovsan, J., Kachko, I., Ovadia, H. and Rudich, A. (2009) Positive and negative regulation of insulin signaling by reactive oxygen and nitrogen species. *Physiol. Rev.*, **89**, 27–71.
37. Brand, M.D. and Nicholls, D.G. (2011) Assessing mitochondrial dysfunction in cells. *Biochem. J.*, **435**, 297–312.
38. Heinonen, S., Buzkova, J., Muniandy, M., Kaksonen, R., Ollikainen, M., Ismail, K., Hakkarainen, A., Lundbom, J., Lundbom, N., Vuolteenaho, K. *et al.* (2015) Impaired

mitochondrial biogenesis in adipose tissue in acquired obesity. *Diabetes*, **64**, 3135–3145.
39. Jheng, H.F., Tsai, P.J., Guo, S.M., Kuo, L.H., Chang, C.S., Su, I.J., Chang, C.R. and Tsai, Y.S. (2012) Mitochondrial fission contributes to mitochondrial dysfunction and insulin resistance in skeletal muscle. *Mol. Cell. Biol.*, **32**, 309–319.
40. Liu, G., Park, S.H., Imbesi, M., Nathan, W.J., Zou, X., Zhu, Y., Jiang, H., Parisiadou, L. and Gius, D. (2017) Loss of NAD-dependent protein deacetylase sirtuin-2 alters mitochondrial protein acetylation and dysregulates mitophagy. *Antioxid. Redox Signal.*, **26**, 849–863.
41. Zorzano, A., Liesa, M. and Palacin, M. (2009) Mitochondrial dynamics as a bridge between mitochondrial dysfunction and insulin resistance. *Arch. Physiol. Biochem.*, **115**, 1–12.
42. Jiang, W., Wang, S., Xiao, M., Lin, Y., Zhou, L., Lei, Q., Xiong, Y., Guan, K.L. and Zhao, S. (2011) Acetylation regulates gluconeogenesis by promoting PEPCK1 degradation via recruiting the UBR5 ubiquitin ligase. *Mol. Cell*, **43**, 33–44.
43. Lin, R., Tao, R., Gao, X., Li, T., Zhou, X., Guan, K.L., Xiong, Y. and Lei, Q.Y. (2013) Acetylation stabilizes ATP-citrate lyase to promote lipid biosynthesis and tumor growth. *Mol. Cell*, **51**, 506–518.
44. Szegő, É.M., Gerhardt, E. and Outeiro, T.F. (2017) Sirtuin 2 enhances dopaminergic differentiation via the AKT/GSK-3b/b-catenin pathway. *Neurobiol. Aging*, **56**, 7–16.
45. Belman, J.P., Bian, R.R., Habtemichael, E.N., Li, D.T., Jurczak, M.J., Alcazar-Roman, A., McNally, L.J., Shulman, G.I. and Bogan, J.S. (2015) Acetylation of TUG protein promotes the accumulation of GLUT4 glucose transporters in an insulin-responsive intracellular compartment. *J. Biol. Chem.*, **290**, 4447–4463.
46. Wang, R.H., Kim, H.S., Xiao, C., Xu, X., Gavrilova, O. and Deng, C.X. (2011) Hepatic Sirt1 deficiency in mice impairs mTorc2/Akt signaling and results in hyperglycemia, oxidative damage, and insulin resistance. *J. Clin. Invest.*, **121**, 4477–4490.
47. Lu, M., Sarruf, D.A., Li, P., Osborn, O., Sanchez-Alavez, M., Talukdar, S., Chen, A., Bandyopadhyay, G., Xu, J., Morinaga, H. *et al.* (2013) Neuronal Sirt1 deficiency increases insulin sensitivity in both brain and peripheral tissues. *J. Biol. Chem.*, **288**, 10722–10735.
48. Cha, Y., Han, M.J., Cha, H.J., Zoldan, J., Burkart, A., Jung, J.H., Jang, Y., Kim, C.H., Jeong, H.C., Kim, B.G. *et al.* (2017) Metabolic control of primed human pluripotent stem cell fate and function by the miR-200c-SIRT2 axis. *Nat. Cell Biol.*, **19**, 445–456.
49. Biddinger, S.B. and Kahn, C.R. (2006) From mice to men: insights into the insulin resistance syndromes. *Annu. Rev. Physiol.*, **68**, 123–158.
50. Tan, Y., Ichikawa, T., Li, J., Si, Q., Yang, H., Chen, X., Goldblatt, C.S., Meyer, C.J., Li, X., Cai, L. *et al.* (2011) Diabetic downregulation of Nrf2 activity via ERK contributes to oxidative stress-induced insulin resistance in cardiac cells in vitro and in vivo. *Diabetes*, **60**, 625–633.
51. Liew, C.C., Ma, J., Tang, H.C., Zheng, R. and Dempsey, A.A. (2006) The peripheral blood transcriptome dynamically reflects system wide biology: a potential diagnostic tool. *J. Lab. Clin. Med.*, **147**, 126–132.
52. Oliver, P., Reynes, B., Caimari, A. and Palou, A. (2013) Peripheral blood mononuclear cells: a potential source of homeostatic imbalance markers associated with obesity development. *Pflügers Arch.*, **465**, 459–468.
53. Bonora, E., Targher, G., Alberiche, M., Bonadonna, R.C., Saggiani, F., Zenere, M.B., Monauni, T. and Muggeo, M. (2000) Homeostasis model assessment closely mirrors the glucose clamp technique in the assessment of insulin sensitivity: studies in subjects with various degrees of glucose tolerance and insulin sensitivity. *Diabetes Care*, **23**, 57–63.
54. Matthews, D.R., Hosker, J.P., Rudenski, A.S., Naylor, B.A., Treacher, D.F. and Turner, R.C. (1985) Homeostasis model assessment: insulin resistance and beta-cell function from fasting plasma glucose and insulin concentrations in man. *Diabetologia*, **28**, 412–419.
55. Ramos, E. and Barros, H. (2007) Family and school determinants of overweight in 13-year-old Portuguese adolescents. *Acta Paediatr.*, **96**, 281–286.
56. Ohkawa, H., Ohishi, N. and Yagi, K. (1979) Assay for lipid peroxides in animal tissues by thiobarbituric acid reaction. *Anal. Biochem.*, **95**, 351–358.